

Investigation of nanostructured Pd–Ag/n-ZnO thin film based Schottky junction for methane sensing

S. Roy¹ · S. Das¹ · C. K. Sarkar²

Received: 6 January 2016 / Accepted: 30 June 2016 / Published online: 7 July 2016
© The Author(s) 2016. This article is published with open access at Springerlink.com

Abstract Undoped nanocrystalline n-type ZnO thin film was deposited by chemical deposition technique on a thermally oxidized p-Si ($\sim 5 \Omega \text{ cm}$ resistivity and $\langle 100 \rangle$ orientation) substrate. Formation of stable zinc oxide thin film was confirmed by two-dimensional X-Ray Diffraction (XRD) and EDX analysis. The average crystallite size of the ZnO sample was evaluated as $\sim 50 \text{ nm}$. The surface was characterized by Field Emission Scanning Electron Microscopy (FESEM) and Atomic Force Microscopy (AFM) that confirm the formation of nanocrystalline (grain size $\sim 50 \text{ nm}$) ZnO thin film with surface roughness of $\sim 100 \text{ nm}$. Good conversion of precursor into ZnO thin film in the chemical deposition method was evident by Fourier Transform Infrared Spectroscopy (FTIR). A small peak at 479 cm^{-1} was observed in the FTIR spectrum confirming the formation of quartzite structure of the ZnO. The band gap ($\sim 3.44 \text{ eV}$) of the material was calculated from the optical absorption spectroscopy. To prepare Pd–Ag/n-ZnO Schottky junction, Pd–Ag contacts were taken by electron beam evaporation method. I–V characteristics of the junction were studied at different temperatures in inert and reducing ambient (N_2 and $\text{N}_2 + \text{CH}_4$) with turn on voltage of around 0.2 V . The parameters like ideality factor (η), saturation current (I_0), series resistance (R_s), and barrier height (Φ_{BO}) of the junction were calculated in the

temperature range $50\text{--}200 \text{ }^\circ\text{C}$ in N_2 as well as in 1% $\text{CH}_4 + \text{N}_2$ ambient. It was observed that the ideality factor decreases in the temperature range $50\text{--}200 \text{ }^\circ\text{C}$ ($\eta = 12.34$ at $50 \text{ }^\circ\text{C}$ and $\eta = 1.52$ at $200 \text{ }^\circ\text{C}$) in N_2 ambient and $\eta = 1.18$ in $\text{N}_2 + \text{CH}_4$ ambient at $200 \text{ }^\circ\text{C}$. Schottky Barrier Height (Φ_{BO}) of the Pd–Ag/n-ZnO junction was found to increase with temperature. A close observation of Pd–Ag/n-ZnO junction in the presence of methane was performed to appreciate its application as methane sensor. The sensing mechanism was illustrated by a simplified energy band diagram.

Keywords Zinc oxide · Chemical deposition · Pd/Ag contact · Schottky junction · Reducing gas

Introduction

Semiconducting metal oxide is receiving vast applications in toxic and inflammable gas sensing, optoelectronics like solar cells, ultraviolet laser emission, photodetectors, short wave length light-emitting diode, transparent electrode display, piezoelectricity, biosensors etc. [1–7]. Among them Zinc Oxide (ZnO) (II–VI wide band gap semiconductor) is much more popular as it has direct band to band transition (3.44 eV) at low temperature and 3.3 eV at room temperature, and its excitonic binding energy is 60 meV signifying that the electron–hole pairs are more stable at room temperature as thermal energy required at room temperature to break one covalent bond is 25 meV . Among these parameters lattice matching between the deposited material and the substrate greatly affects the crystal growth of the deposited material. Presently several nanoforms of ZnO like rods, combs, rings, springs, wires, belts [8–12], and propellers are becoming popular in the ultra-sensitive

✉ S. Roy
sunipa_4@yahoo.co.in

¹ IC Design and Fabrication Center, Department of Electronics and Telecommunication Engineering, Jadavpur University, Kolkata 700032, India

² Nano Device Simulation Laboratory, Department of Electronics and Telecommunication Engineering, Jadavpur University, Kolkata 700032, India

nano-sized gas sensors and in the field of optoelectronics for their interesting properties compared to their bulk counterpart.

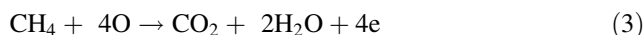
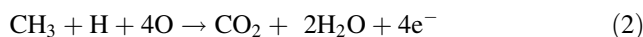
Therefore, a precise knowledge about its structural and optical behavior is essential for making different microelectronics devices. ZnO thin films are prepared by various techniques like chemical vapor deposition, pulsed laser deposition, spray pyrolysis, electrochemically grown technique, galvanic method, sol–gel method, and chemical bath deposition, etc. [13–21]. Amongst these different available techniques, chemical deposition technique is advantageous as it is easy to deposit and requires lower operating temperature (150–200 °C) than sol–gel, vapor phase technique. Substrate temperature is also a key factor for the growth of nanocrystalline thin film particularly for vapor phase technique as higher substrate temperature prevents the crystallographic orientation of the required material as it causes agglomeration of the material. But the drawback is that it needs sophisticated equipment whereas chemical deposition process can be carried out with less expensive and uncomplicated equipment producing minimal waste.

During or after nanostructure synthesis, the surfaces can be easily contaminated by impurities and other defects, e.g. surface defects such as hydroxyl quenches which prevents efficient charge transfer between ZnO and the adsorbed molecules at the interfaces due to which the sensitivity of the device becomes retarded and also the quantum efficiency of optoelectronic devices are reduced [22–24]. The optical and structural properties are also dependent on preparation techniques, type of substrate, lattice matching with the substrate, substrate temperature, and annealing behavior.

This work reports the synthesis of ZnO thin film by chemical deposition technique and the structural characterizations by X-ray diffraction (XRD, field emission scanning electron microscopy (FESEM), and atomic force microscopy (AFM) that gives us the crystallographic orientation, surface morphology and grain structure. Optical characterization is done by UV–Vis spectroscopy that provides us optical characteristics such as band gap energy from absorption spectra, defect luminescence, etc. Also, we have investigated the impurities and defects present in the as deposited sample by Fourier Transform Infrared Spectroscopy (FTIR spectroscopy). The role of defects and impurities are understood by UV–Vis spectroscopy.

Metal oxides (ZnO in this case) help the low-temperature dissociation of methane molecules. Methane is called ‘Fire damp,’ applicable for underground coal mines and has a tendency to explode. Moreover, it may cause breathing problem by producing CO₂ while eliminating oxygen from air. Therefore, proper understanding of its behavior when it comes into metal–semiconductor contact is crucial for the fabrication of an ideal methane sensor.

The semiconducting nanostructures with smaller dimensions are having increased molar free energy and, therefore, are more susceptible to adsorption of molecules onto their surfaces. The dissociation of methane can be depicted as follows:



As these nanostructures have higher adsorption coefficient for gases, the adsorption of reducing gases happens easily onto the nanocrystalline metal oxide surface.

Zheng et al. [25] studied the relationship between the oxygen defect and the photocatalytic property of Ag/ZnO heterostructure. Wu and Tseng [26] studied the influence of different diameters and densities of the nc-Au on the photocatalytic activity in Au/ZnO nanorod composites. Recently, Basu et al. [27] reported on lowering the sensing temperature further to ~100 °C with surface modified (by Pd nanoparticles dispersion) ZnO thin films deposited by electrochemical process. But the limitation of this process is its incompatibility to standard CMOS process technology. Bhattacharyya et al. [28] reported on ZnO thin film hydrogen sensor developed by sol–gel process. Sol–gel process, in spite of its CMOS compatibility, suffers from the incorporation of a high-temperature (600–800 °C) processing step. Mishra et al. [29] explored the effect of catalytic metal contact on methane sensing performance of n-ZnO/p-Si heterojunction with four different types of sensor structure emphasizing the fact that the presence of noble metal highly modulates the sensor characteristics as it enhances the hydrogen adsorption by lowering the activation energy needed to start the experiment. Basu et al. [30] compared the types of ZnO sensor structure Pd–Ag/ZnO/Zn and Rh/ZnO/Zn (MIM) obtained from electrochemical anodization method in the absence and presence of UV light. The optimum temperature and the optimum voltage for methane sensing were found 220 °C and 0.4 V, respectively. The undoped zinc oxide thin films grown under UV light offered better performance for methane sensing, but the limitation of this process is again lack of CMOS process compatibility.

Schottky junctions are formed by depositing a metal over the lightly doped semiconductor where $\Phi_m > \Phi_s$, Φ_m is the metal work function and Φ_s is the semiconductor work function. The current flow in a Schottky diode is due to the transport of majority carriers only. When the metal and n-type semiconductors are brought into contact, electrons from the semiconductor move out to flow into the lower energy states of the metal until the Fermi levels are aligned. As electrons flow to the metal side, positively charged fixed donor ions are left behind in the n type

semiconductor forming a depletion layer which opposes the flow of electron from the semiconductor to the metal initiating a band bending across the junction to keep the Fermi level flat.

In the present study, to explore the catalytic effect of Pd–Ag (70 %) contact, Schottky junction characteristics were investigated in the temperature range of 50–200 °C in nitrogen and also methane with nitrogen. The formation of n-ZnO was unintentional and might be due to the presence of oxygen vacancies in the bulk.

After dissociation of methane, hydrogen molecules are adsorbed on the ZnO surface from the surrounding ambient and as a result its work functions changes. The barrier height of the Pd–Ag/n-ZnO junction also changes. Therefore, the conductivity of the ZnO layer changes. I–V characteristic of the metal–semiconductor Schottky junction is essentially the same as that of ordinary p–n junction though the physical mechanism involved is more complicated. The current in the schottky junction is mainly due to the majority carriers.

According to metal–semiconductor junction theory, there are three different theories of current conduction. The first one is diffusion theory which deals with the diffusion of carriers from the semiconductor into the metal if metal work function is greater than semiconductor work function. The diffusion current density is a function of the minority carrier diffusion length and the applied junction voltage. The driving force is distributed along the length of depletion layers. According to diode theory, saturation current (I_0) depends on temperature and barrier height, whereas diffusion theory gives the concept that the saturation current also depends on applied voltage to certain extent [23]. The second one is thermionic emission theory which is temperature dependent and proposes that the carriers which have energy equal to or larger than the conduction band energy at the metal–semiconductor interface contribute to the current flow across the Schottky junction; and the third one is quantum–mechanical tunneling through the Schottky barrier which suggests that as the doping concentration increases, the probability of tunneling through the barrier increases. Typically, only one current flow mechanism dominates based on the above theories.

As already established, the diffusion and thermionic emission currents can be written in the following form [24]:

$$J_n = qvN_c \exp\left(\frac{-\Phi_{B0}}{V_t}\right) \left[\exp\left(\frac{V_a}{V_t}\right) - 1 \right] \quad (4)$$

This equation states that the current is the product of the electronic charge q , a velocity v , and N_c the density of available charge carriers in the metal–semiconductor interface. Φ_{B0} is the Schottky barrier height that is equal to the difference between the Fermi level in the metal

($E_{F_{Pd-Ag}}$ in this case) and the conduction band edge E_c of metal oxide (in this case ZnO) assessed at the interface of the metal– semiconductor junction. V_a is nothing but the applied voltage. Negative sign is used to ensure that no current will flow when the applied voltage is zero because in thermal equilibrium any flow of carriers is counterbalanced by the flow of carriers in opposite direction.

Similarly, the tunneling current can be expressed as [24] follows:

$$J_n = qV_R n^\theta, \quad (5)$$

where V_R is the Richardson velocity and J_n is the density of carriers in the semiconductor. The term n^θ is called tunneling probability which shows the dependency of total current on the carrier flux arriving at the tunnel barrier multiplied with the probability n^θ , at tunnel through the barrier.

In this case, Pd–Ag/n-ZnO junction characteristics were explained by thermionic emission theory. Series resistance (R_s) is another important parameter for the Pd–Ag/n-ZnO Schottky junction to observe its electrical behavior [12]. From the Schottky diode current–voltage relationship, the junction parameters of Pd–Ag/n-ZnO interface like ideality factor (η), saturation current (I_0), series resistance (R_s), and barrier height (Φ_{B0}) were calculated in the given temperature range (50–200 °C) in N_2 ambient and $CH_4 + N_2$ ambient. Experiments in N_2 ambient were deliberately considered to avoid the susceptibility of oxygen on the interface properties.

Experimental

Thin film deposition

Nanocrystalline undoped n-ZnO thin films were deposited on SiO_2/p -Si substrates (1–5 Ω cm, 5 × 5 mm) by a low-cost chemical deposition technique whose details were published in our earlier publication [13]. Complete flowchart of the preparation of nanocrystalline n-ZnO thin film by chemical deposition method is given in Fig. 1.

Crystallinity, morphology, optical, and electrical studies

The information of the samples was investigated using X-ray diffractometry (XRD), EDX, FESEM, UV–vis absorption spectroscopy (UV–vis), FTIR spectroscopy.

X-ray Diffraction (ULTIMA-III, Cu $K\alpha$ target, X-Ray Diffractometer) was carried out to estimate the crystal structure, crystallite size, and crystal orientation of chemically deposited ZnO thin film. Energy dispersive X-ray scattering EDX ((EDX; Jeol JSM-6X60La, emitter

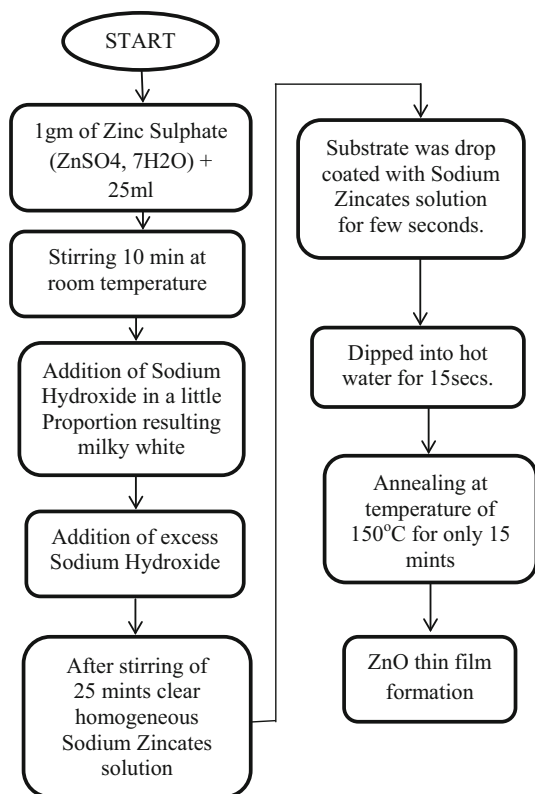


Fig. 1 Process flowchart of ZnO preparation

voltage = 20 kV and emitter current = 20 μ A) was employed to study the chemical composition of the deposited ZnO thin films. Scanning Electron Microscopy (FESEM; JEOL, JSM-6700F used emitter voltage = 5 kV and emitter current = 10 μ A) and Atomic Force Microscopy (Veeco Model: Dimension 3100 Nanoman) were employed to reveal the micro structure and to study the surface morphology of ZnO thin film. FTIR spectroscopy is a very useful method for examining the vibrational properties of any synthesized material. FTIR spectroscopy was done by Shimadzu IR Prestige 21 spectrophotometer in the interval of wave number of 400–4000 cm^{-1} .

Perkin Elmer Lambda 35 instrument was used to measure the optical absorption spectra. The n-type conductivity of the ZnO thin film was verified by the well-known hot probe method.

Schottky contact formation

Pd–Ag was chosen to avoid palladium hydride formation as this may be the case with Pd only due to the phase transition. Pd–Ag electrodes of 1×1 mm dimension, thickness 0.2 μm , and separation of 1 mm were deposited on the surface of ZnO thin film, by e-beam evaporation using an Al shadow mask. Immediately after deposition, electrical contacts were taken by using fine copper wire and room

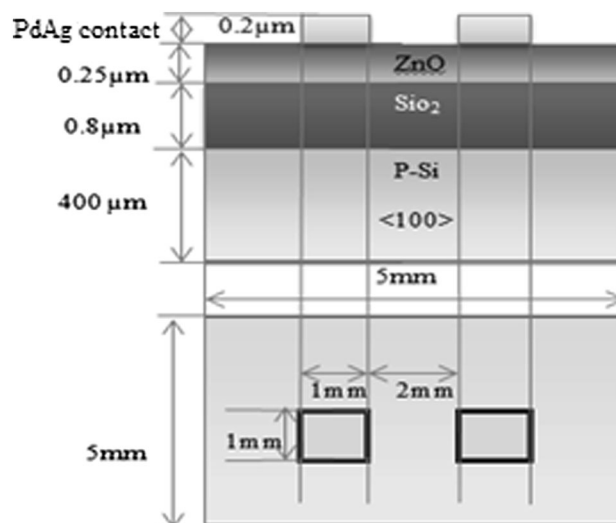


Fig. 2 Schematic of the device

temperature silver paste. The cross-sectional as well as the top view of the planar device is shown in Fig. 2.

I–V characteristic measurement set up

To study the effect of Pd–Ag/n-ZnO Schottky junction at different temperatures, a setup consisting of a cylindrical corning glass chamber (length 25 cm and diameter 3.5 cm) with inlet and outlet for gases was placed horizontally and coaxially inside a resistively heated furnace with a 4 cm constant temperature zone. IOLAR grade N₂ was used as the carrier gas for ultra pure methane, which is mixed in proportion in a chamber followed by a mixing coil. The gas flow and mixing ratio were precisely monitored and controlled with the help of mass flow controller (MFC) (Alicat scientific, M-50SCCM-D) for methane and a needle valve and mass flow meter (MFM) (Alicat scientific, M-1000SCCM-D) for N₂. During the testing, the gas pressure on the sensor was 1 atm. The current–voltage characteristics were studied by a Fluke pico-ammeter-voltage source (model: 8845A/8846A). Each experiment was repeated with two samples of same dimension and the maximum variation from the optimized result of about ± 3 % was recorded. The samples are exposed to N₂ and then to 1 % CH₄ in N₂ in the temperatures range 50–200 $^{\circ}\text{C}$.

Result and discussion

Structural characterization

X-ray diffraction (XRD) analysis

The XRD pattern of this sample is shown in Fig. 3. From this diffraction pattern, it is observed that there is a significant as well as strong reflection peak corresponding to

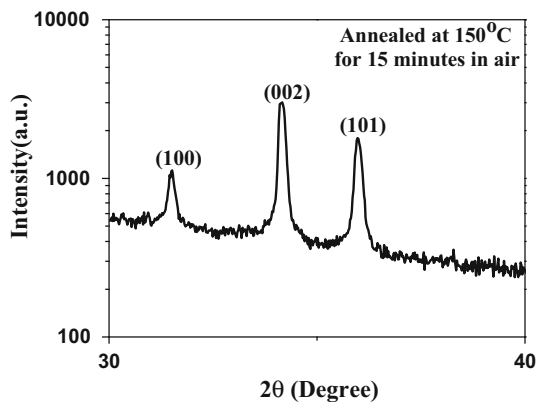


Fig. 3 XRD spectra of ZnO thin film

(002) crystal plane. This peak confirms perfect c-axis orientation. Other reflection peaks having descending intensities are obtained corresponding to (101), (100) and (103) planes, respectively. The Bragg’s angle corresponding to (002), (100), and (101) planes are 34.19°, 31.55°, and 35.93°, respectively. The interplaner spacing (*d*) is calculated by using Bragg’s formula [24]:

$$2d \sin\theta = n\lambda \tag{6}$$

The crystal structure is estimated by using the following equation [24]:

$$\frac{1}{d^2} = \left(\frac{4}{3}\right) \left\{ \frac{(h^2 + k^2 + hk)}{a^2} \right\} + \left(\frac{l^2}{c^2}\right) \tag{7}$$

As we have two most significant peaks corresponding to (002) and (100) plane, we only use the Miller indices of these planes to calculate the lattice parameters. Using (002) plane, the calculated value of lattice parameter ‘*c*’ is found to be 5.2388 Å. The interplaner spacing ‘*d*’ = 2.6194 Å corresponding to Bragg’s angle (2θ) = 34.19° is used. Lattice parameter ‘*a*’ is found to be 3.27 Å taking (100) plane where the value of *d* is 2.8323 Å. The *c/a* value is estimated as 1.6020 which confirms Hexagonal Wurtzite structured ZnO.

The crystallite size (*D*) is calculated by using Scherrer’s formula [24]:

$$D = \frac{K\lambda}{\beta \cos\theta}, \tag{8}$$

where *K* is called Scherrer’s constant (0.9), and λ is the wavelength of emitted X-ray; here $\lambda = 1.54 \text{ \AA}$ for Cu $K\alpha$

target. β is the full width at half maxima (FWHM) and θ is half of the Bragg’s angle.

For (002) plane the calculated crystallite size is 41.06 nm that confirms the deposited material is nanomaterial. The calculated grain size for all the reflecting planes is shown in Table 1.

Dislocation Density (length of Dislocation line per unit volume) is calculated using Williamson–Smallman relation [24]

$$\delta = \frac{1}{D^2}, \tag{9}$$

where *D* is the crystallite size. Strain of the thin film is estimated by using Williamson–Hall equation [24]:

$$(\beta^2 - \beta_0^2) \cos 2\theta = (4\epsilon \sin\theta)^2 + \frac{0.9\lambda^2}{D^2} \tag{10}$$

where ϵ strain of the material due to grain boundary and strain is calculated as $\epsilon = \beta/4\tan\theta$ and $\beta_0 = 0.05$.

Zn–O bond length (*L*) is calculated by using the following formula [24]:

$$L = \left[\frac{a^2}{3} + \left(\frac{1}{2} - u\right)^2 c^2 \right], \tag{11}$$

where the parameter *u* in the wurtzite structure, $u = \frac{a^2}{3c^2} + 0.25$. From this, the estimated Zn–O bond length was found to be 3.65 Å.

The average crystallite size of the ZnO sample was evaluated as ~48.31 nm for the (100) plane, ~47.61 nm for the (101) plane, and ~38.61 nm for the (103) plane, as confirmed by JCPDS card (JCPDS-ICDD PDF no: 46-1043).

Morphological study

FESEM study and EDX analysis

Field Emission Scanning Electron Microscopy is used to prove the formation of nanocrystalline ZnO (Fig. 4.) Prior to insertion in the sample chamber of the scanning electron microscope, the ZnO thin film was coated with a thin ($\gg 100 \text{ \AA}$) layer of Gold (Au) to avoid charging effects. The average crystal size and pore size both are indicated in the FESEM micrograph.

Table 1 Crystallite size for different reflecting planes

Planes	2θ (°)	Interplaner spacing (Å)	FWHM (β) ($\times 10^{-3}$ rad)	Crystallite size (<i>D</i>) (nm)	δ ($\times 10^{14}$) lines/m ²	ϵ ($\times 10^{-3}$)
(100)	31.55	2.8323	2.98	48.31	4.284	2.64
(002)	34.185	2.6198	3.48	41.06	5.931	2.83
(101)	35.93	2.4965	3.06	47.61	4.411	2.36
(103)	62.67	1.4806	4.18	38.60	6.712	1.72

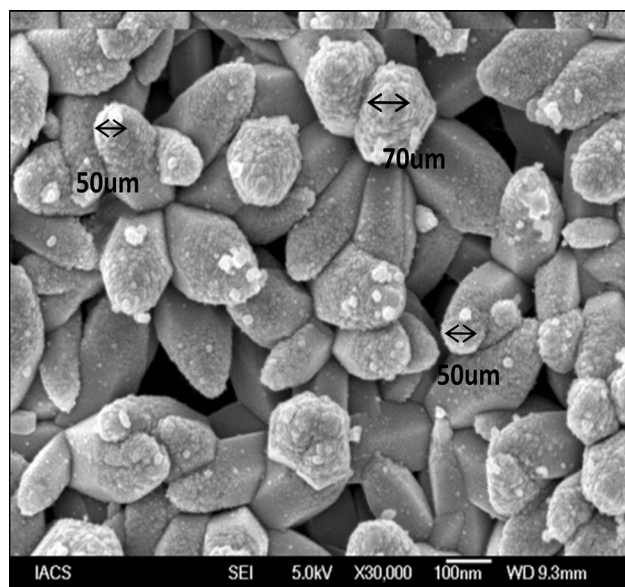


Fig. 4 FESEM image of ZnO thin film

The FESEM micrograph explores the hexagonal needle-like structures having dimension of $\sim 50\text{--}70$ nm with average pore diameter of ~ 80 nm. The non-uniform heating of the ZnO samples may be the possible cause of different particle size.

The Surface roughness of the as deposited thin film is observed by atomic force microscopy. From the AFM image peak-to-valley roughness ($Z_{\max} - Z_{\min}$) is found to be about 100 nm. The peak-to-valley roughness is calculated from the distance between the highest peak (Z_{\max}) and the lowest valley (Z_{\min}) of the measured surface. The vertical height of the surface is denoted here by Z .

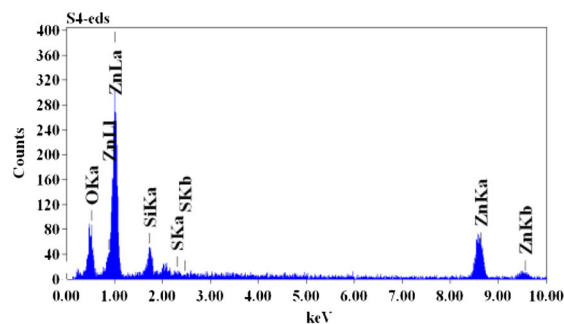
Energy dispersive X-ray scattering EDX was employed to study the chemical composition of the deposited ZnO thin films. The non-stoichiometric nature of Zinc Oxide was established by the EDX analysis (Fig. 5).

Thickness of the film (ZnO) was found $0.2574\ \mu\text{m}$ (measurement was carried out by Taylor Hobson Ultra-Surface 602-1 software).

Optical characterization (impurity perspective)

FTIR spectroscopy study

Fourier Transform Infra-Red (FTIR) spectroscopy is employed to identify organic or inorganic chemical present in the sample, which is attributed to different functional groups corresponding to different absorbance peaks in the spectra. When the sample is irradiated by infrared light there is a transition between two vibrational levels (found from Schrodinger equation), manifesting the molecules present in that sample. FTIR spectroscopy was done by



Ele...	Cl...	(keV)	mass%	Error%	At%
O	K	0.525	24.78	0.56	53.80
Si	K	1.739	7.70	0.39	9.53
S	K	2.307	1.44	0.28	1.56
Zn	K	8.630	66.08	1.60	35.11
Total			100.00		100.00

Fig. 5 EDX spectra of ZnO thin film

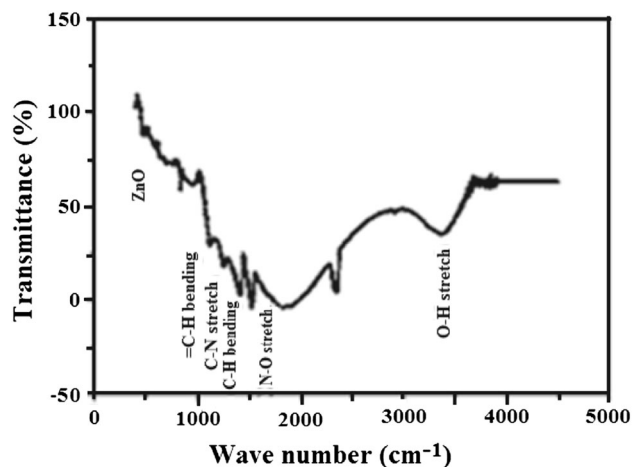


Fig. 6 FTIR analysis of ZnO thin film

Shimadzu IR prestige 21 spectro-photometer with the wave number of $400\text{--}5000\ \text{cm}^{-1}$. Figure 6 shows the FTIR spectra of as deposited ZnO thin film. A series of absorption peaks were observed from 400 to $4500\ \text{cm}^{-1}$. A strong and broad peak was obtained at $3376.27\ \text{cm}^{-1}$ indicating that the presence of hydroxyl group (O–H stretch, H-bonded) may be due to the hygroscopic character of ZnO. Some undefined peaks may be observed in the spectra which do not represent any functional group, so they may be considered as noise. A sharp and strong peak near $1560\ \text{cm}^{-1}$ represents N–O stretch. Another sharp and strong peak present in the spectra at $1417\ \text{cm}^{-1}$ is due to C–H bending. A small peak near $1250\ \text{cm}^{-1}$ represents C–N stretch and a strong peak at $844\ \text{cm}^{-1}$ represents = C–H bending. A small peak in close proximity of $437\ \text{cm}^{-1}$, at $479\ \text{cm}^{-1}$, is for E2 mode or the high-frequency phonon

mode of RAMAN spectra of ZnO, which confirms the formation of wurtzite structure of the ZnO. Therefore, it may be concluded that 479 cm^{-1} is the Zn–O bond frequency.

Here, we have found impurities like hydroxyl(O–H), Nitro(N–O), Alkane(C–H), Amine(C–N), and Alkene(=C–H). Hydroxyl group may be generated in this sample due to reaction of produced ZnO with HCl which is used to clean the apparatus or due to the hygroscopic nature of ZnO. Nitro group is possibly formed due to Zn with HNO_3 that is used to clean the oxidized wafer. Alkane and Alkene group can be produced due to Acetone (CH_3COCH_3) wash of the oxidized wafer. Amine group may be formed during the synthesis process.

UV–Vis spectroscopy

UV–Vis spectroscopy is employed to determine the optical energy band gap, position of defect states due to contamination, and the luminescence of these defect states of a transparent material. Actually, this study reveals the transition of atoms or molecules (most probable transition is from HOMO (Highest occupied molecular orbital) state to LUMO (Lowest unoccupied molecular orbital) state) when they are irradiated by ultraviolet and visible region of electromagnetic spectrum. We have performed this spectroscopy by PERKIN ELMER λ 35. In this sample, the dependence of absorption of the films (deposited on SiO_2/Si substrate) on wavelength is shown in Fig. 7a. Strongest absorption occurs in the UV wavelength at 362 nm. Broad and strong trough is developed at 534 nm in the visible range and a step increment of absorption occurs at 561 nm. After that, there is a sustainable absorption. This peak corresponding to this energy value is the envelope of phonon replicas of free exciton luminescence. As there is a sudden fall in absorbance at 534 nm corresponding 2.3 eV, it may be concluded that our sample has low Green defect luminescence which might be due to oxygen vacancy.

Energy band gap E_g and absorption coefficient α is related by the following equation [24]:

$$(\alpha h\nu) = K(h\nu - E_g)^\beta, \tag{12}$$

where $h\nu$ is the incident photon energy and β is characterization factor determining the electronic transition between valence band and conduction band $\beta = 1/2$ for direct band gap semiconductor.

As ZnO is direct band gap semiconductor, in this case the Eq. (12) becomes

$$(\alpha h\nu) = K_B(h\nu - E_g)^{\frac{1}{2}} \tag{13}$$

$$\text{Thus } E_g = h\nu - \frac{(\alpha h\nu)^2}{K_B^2} \tag{14}$$

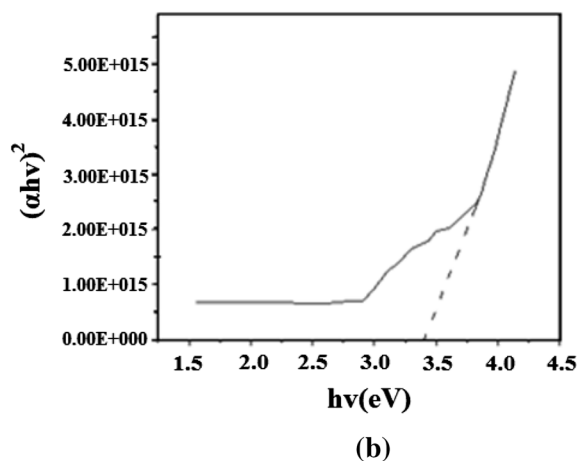
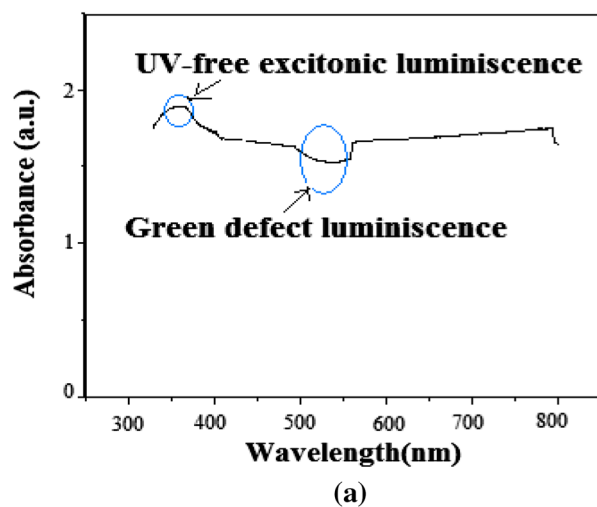


Fig. 7 a Transmittance spectra of ZnO thin film, b $(\alpha h\nu)^2$ vs $h\nu$ plot of ZnO thin film

K_B the Boltzmann constant (1.38×10^{-23} J/K), and h is the Planck constant (6.62×10^{-34} J-s). The effective Richardson constant for n-ZnO as obtained from literature is $A^{**} = 24\text{ A/cm}^2\text{K}^2$ [31]. The band gap of this film corresponding to the highest peak can be calculated using Tauc’s procedure where $(\alpha h\nu)^2$ was plotted against $h\nu$ and extrapolating the linear portion of absorption edge to the energy axis (straight line portion) which is exhibited in Fig. 7b. The measured value of band gap energy of ZnO thin film is 3.326 eV. Here α is called absorption coefficient of the ZnO thin film that is calculated using the following expression [24]:

$$\alpha = \frac{2.303A}{t}, \tag{15}$$

where A is the absorbance measured from spectra for highest peak and t is the thickness of the film. In this case, A was found at 1.89 a.u. and t is 257.4 nm. The absorption

coefficient α becomes 1.69×10^9 in UV region and 1.43×10^9 in visible region. The relatively lower adsorption coefficient of the film gives support to ZnO transparency in visible region. α is also related with extinction coefficient K by [24]

$$K = \frac{\alpha\lambda}{4\pi}, \quad (16)$$

where λ is the wavelength of the incident radiation $= c/\nu$; ν is the frequency of the incident photon; and $c = 3 \times 10^8$ m/s.

Using Eq. (14), the calculated band gap energy of ZnO thin film becomes 3.44 eV that is in close proximity of theoretical value (3.3 eV).

Effect of methane on Pd–Ag/n–ZnO Schottky Junction

Nanocrystalline materials offer higher surface to volume ratio than bulk. When the crystal size is decreasing, more and more surface is exposed and the fraction of atoms at the grain boundary increases. Due to some inherited defects (or nodes), grain boundaries contain vacancies/dangling bonds at the surface. Gas interaction process is mainly a charge transfer phenomenon. As the number of nodes increases at the surface, current conduction capabilities of the surface increase as well.

The forward current–voltage characteristics of the Pd–Ag/n–ZnO Schottky contact in the temperature range 50–200 °C, in nitrogen and in the presence of methane in nitrogen, respectively, are shown in Fig. 8.

The relation between applied bias voltage and the forward and reverse current through the Pd–Ag/n–ZnO Schottky junction with uniformly thin oxide layer follows the thermionic emission theory enabling the transport of electrons over the potential barrier from semiconductor (ZnO) to metal (Pd–Ag). It can be seen that the Schottky diode has the typical forward semiconductor diode characteristic, but with a much lower turn on voltage of around 0.2 V. At high current levels, it levels off and is limited by the series resistance or the maximum level of current injection. In the reverse direction, there is a greater level of reverse current than that experienced using a more conventional PN junction diode.

Reverse saturation current for Schottky barrier diode, and a normal PN junction diode, as well as the current conduction mechanisms, are different. In a PN junction diode, the current is due to diffusion of minority carriers, whereas in Schottky diode the current is due to thermionic emission of majority carriers over a potential barrier. As this is highly temperature dependent, a detailed study with respect to temperature is a major subject of concern.

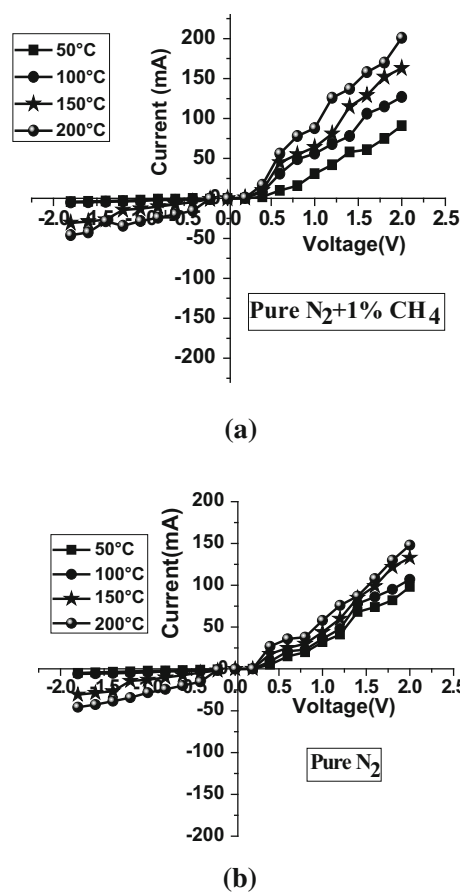


Fig. 8 Forward bias I–V characteristics of Pd–Ag/n–ZnO Schottky junction **a** with gas, **b** without gas

Based on the thermionic emission theory, the ideality factor (η), the Schottky barrier height (Φ_{B0}), the saturation current (I_0), and the series resistance (R_s) of the Pd–Ag/n–ZnO Schottky junction were evaluated using the following equations:

$$I = AA^{**}T^2 \exp\left[-\frac{q\Phi_{B0}}{KT}\right] \left[\exp\left(-\frac{qV}{\eta KT}\right) - 1\right] \quad (17)$$

$$I = I_0 \exp\left[-\frac{qV}{\eta KT} - 1\right] \quad \text{for } V > \frac{3KT}{q} \quad (18)$$

$$I_0 = AA^{**}T^2 \exp\left[\frac{-q\Phi_{B0}}{KT}\right], \quad (19)$$

where A is the contact area, V is the applied voltage drop across the rectifying contact, T is the absolute temperature in Kelvin, and A^{**} is the effective Richardson constant. Saturation current (I_0) can be calculated by extrapolating the linear region of the $\ln I$ - V curve to zero applied voltage.

Ideality factor η determines the departure from the ideal diode characteristics of the metal–semiconductor Schottky junction ($\eta = 1$ for ideal Schottky junction) and it was

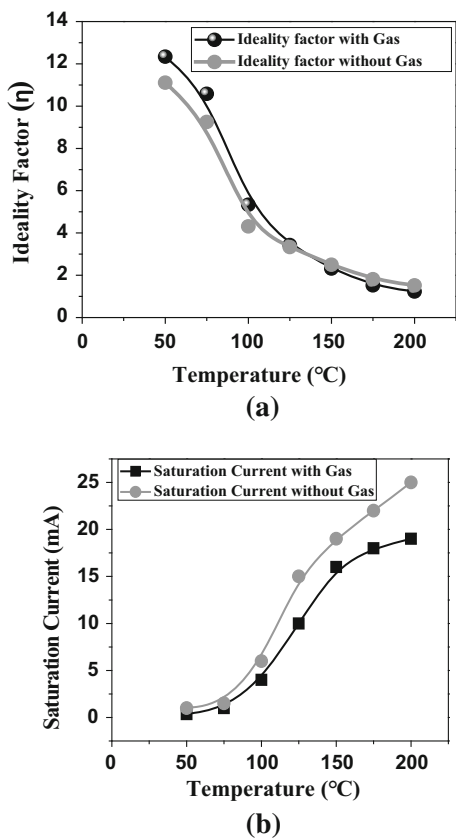


Fig. 9 Variation of **a** ideality factor, **b** saturation current with temperature in both N₂ and 1 % CH₄ in N₂

calculated using the value of the saturation current obtained from Eq. (19).

It was observed from the experimental data (Fig. 9) that the ideality factor of the Pd–Ag/n–ZnO Schottky junction is strongly temperature dependent and inversely proportional to the temperature, i.e. when the temperature increases, the ideality factor decreases in the temperature range 50–200 °C ($\eta = 12.34$ at 50 °C and $\eta = 1.52$ at 200 °C), and the junction becomes almost ideal at 200 °C as shown in Fig. 9a. In the presence of methane gas, ideality factor of the Pd–Ag/n–ZnO Schottky junction follows the same nature yet having lower value compared to that measured in nitrogen ($\eta = 1.52$ in N₂ and $\eta = 1.18$ in N₂ +CH₄ at 200 °C). The possible reason of lowering the ideality factor can be dictated as follows: there is an insulating interfacial layer at the junction formed during annealing as because of diffusion of lattice oxygen to the surface. Because of the possible trapped charges across the junction, the voltage across the oxide is not necessarily zero. A fixed charge density, probably positive, exists across the oxide layer which ultimately affects current through the junction. So current through the junction not only depends on the thermionic emission but also on the tunneling of the trapped charges. At higher temperature it decreases may be due

to the lowering of space charge width in the transition region which is small compared to the carrier diffusion length.

From the diode equation, it is clear that the saturation current increases with increase in temperature (I_0). It was observed that in the presence of methane the value of saturation current was less than the case of without gas. The reason may be as follows: the reduction in barrier height increases the probability of carrier diffusion across the metal semiconductor junction by a factor of $\exp(eV/kT)$ with a tendency to saturate above 200 °C as shown in Fig. 9b.

Barrier height (Φ_{B0}) was calculated from Eq. (20) using the values of the saturation current:

$$\Phi_{B0} = \frac{kT}{q} \ln \left[\frac{AA^{**}T^2}{I_0} \right] \tag{20}$$

Figure 10 shows the curve of barrier height vs temperature. 0.04 cm² contact area (A) was considered for barrier height calculation.

From the above figure, it is clear that Schottky Barrier Height (Φ_{B0}) of the Pd–Ag/n–ZnO junction increases with temperature as expected. Further increase in Φ_{B0} in the presence of methane is probably due to partial passivation of the inter-facial defects.

The zero bias barrier height (Φ_{B0}) increases and the ideality factor (η) decreases with increase in temperature which bear the authenticity of a better Schottky junction.

Series resistance

The forward biased I–V characteristics of real p–n diodes are further affected by high injection and the series resistance of the diode. High injection occurs in the forward biased PN junction when injected minority carrier density exceeds the doping density. High injection occurs first in the lowest doped region of the diode since that region has the highest minority carrier density. When the forward bias

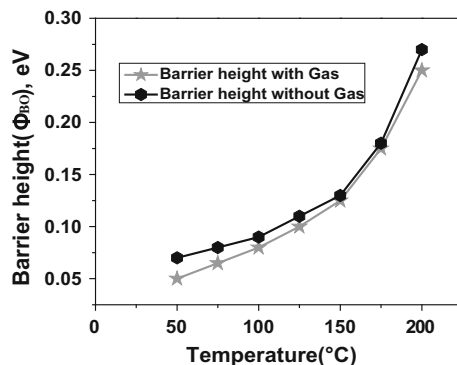


Fig. 10 Variation of barrier height with temperature

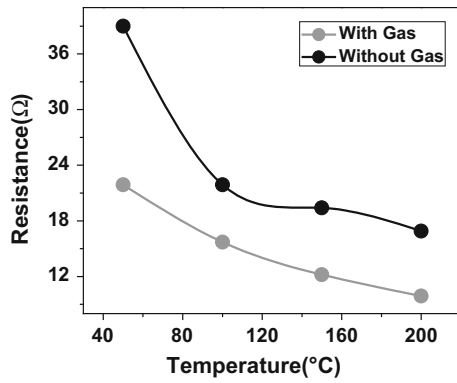


Fig. 11 Variation of series resistance with temperature

is increased, the current will not raise exponentially; rather it increases linearly due to series resistance of the diode. This series resistance may be the sum of contact resistance, inherent defects generated resistance of semiconductor as well as the connecting wires.

From Fig. 11, it was observed that the series resistance decreases with the increase in temperature. It was also noticed that there is an increase in series resistance in the presence of methane, which signifies the improved Pd–Ag/ZnO junction characteristics due to passivation of defects. The decrease of series resistance with temperature is undoubtedly the manifestation of the structural improvement.

Energy band diagram

This section illustrates the behavior of metal–semiconductor rectifying contact or Schottky contact. The ideal energy band diagram for a particular metal and n-type semiconductor after making contact is shown in Fig. 12. The difference in work function of the metal and the semiconductor is mainly responsible for this rectifying nature.

In Schottky contact the current through the metal–semiconductor junction usually depends on the majority carriers. In thermal equilibrium, Fermi level of both metal and semiconductor must be aligned with each other and the valence and the conduction band edge of the n-type semiconductor (n-ZnO) are forced to bend upwards at the interface.

In the above figure, Φ_{Pd-Ag} and $\Phi_{Pd-Ag(G)}$ are, respectively, the work function of Pd–Ag and reduced work function of Pd–Ag in the presence of CH₄ gas. Φ_{ZnO} and $\Phi_{(ZnO)G}$ are the barrier height of Pd–Ag/n-ZnO junction and that is in the presence of CH₄ gas, respectively. $\chi_{(ZnO)}$ is the electron affinity of ZnO. E_C , E_V are the conduction band and the valence band, E_F and E_{FG} are the Fermi level in N₂ and in N₂ + CH₄. Φ_{Pd-Ag} is ~5.51 eV and Φ_{ZnO} is ~4.7 eV found in the literature [32].

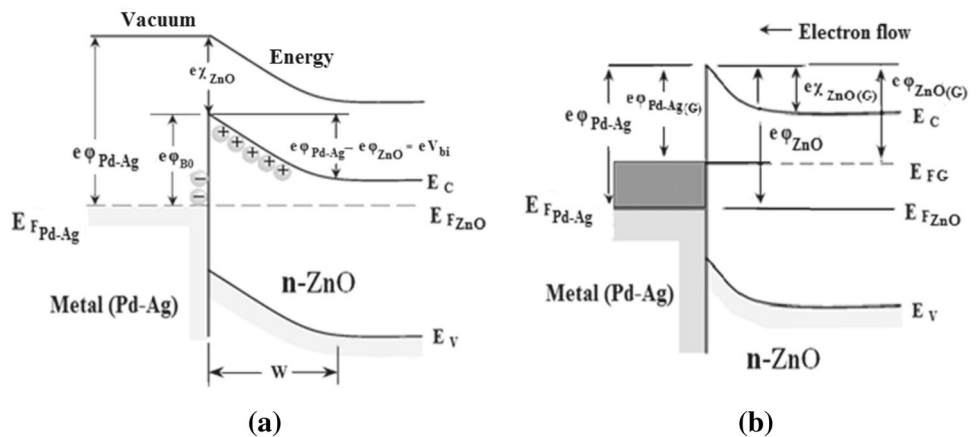
In the present investigation, Pd–Ag/n-ZnO Schottky junction was studied in N₂ ambient and N₂ + 1 % CH₄ ambient to study the effect of methane on the barrier height. From the energy band diagram the barrier height of the Pd–Ag/n-ZnO junction (Φ_{B0}) can be expressed by Eq. (21).

$$\Phi_{B0} = \Phi_{Pd-Ag} - \chi_{(ZnO)} \tag{21}$$

After dissociation of methane, Pd–Ag can adsorb hydrogen on its surface. Consequently, the hydrogen molecules again dissociate from hydrogen atoms on the Pd–Ag surface and get dissolved into the Pd–Ag bulk. These hydrogen atoms on Pd–Ag accept electron from the surface.

As a matter of fact when electrons are removed from the metal surface, work function (Φ_{Pd-Ag}) of the metal (Pd–Ag) is reduced. ($\Phi_{Pd-Ag(G)}$ is the reduced work function in CH₄) and the barrier height of the Pd–Ag/n-ZnO junction is decreased (Fig. 12). As a result, electrons from semiconductor flow into the lower energy states of the metal. Positively charged donor atoms remain in the semiconductor, creating a space charge region. From this figure, it

Fig. 12 a Formation of a Schottky Junction, **b** semiconductor to metal barrier height decreases due to the presence of reducing gas methane (not to scale)



is also apparent that the barrier height of the Pd–Ag/n–ZnO junction, calculated by assuming the thermionic emission theory, is low in the presence of 1 % CH₄ +N₂ compared to pure N₂ ambient at different temperatures.

Conclusions

In this study, a low-cost chemical deposition technique of nanocrystalline zinc oxide thin films on thermally oxidized silicon substrate is reported, and the structural, optical, and electrical properties are studied. Pd–Ag/n–ZnO Schottky junction was tested and the junction properties were meticulously investigated in both nitrogen and in nitrogen mixed with methane. The most fascinating inspection of this report is the modulation of the electrical properties of the junction like ideality factor, series resistance, saturation current, and barrier height in the presence of the reducing gas like methane with proper justification and thus supports the use of Pd–Ag/n–ZnO schottky junction for efficient detection of gases containing hydrogen molecule. Pd–Ag was used to ensure a stable rectifying junction with n type ZnO. Besides, it is popular for its well-known hydrogen adsorbing property which occurs after thermal dissociation of methane in this case.

Acknowledgments Thanks given to DST, Govt of India for financial support. The authors also thankfully acknowledge Prof. H. Saha, former coordinator of IC Centre, ETCE Dept, Jadavpur University, for providing the laboratory facility.

Compliance with ethical standards

Conflict of interest The authors declare that they have no conflict of interest.

Open Access This article is distributed under the terms of the Creative Commons Attribution 4.0 International License (<http://creativecommons.org/licenses/by/4.0/>), which permits unrestricted use, distribution, and reproduction in any medium, provided you give appropriate credit to the original author(s) and the source, provide a link to the Creative Commons license, and indicate if changes were made.

References

1. Yi, G.C., Wang, C., Park, W.: ZnO nanorods: synthesis, characterization and applications. *Semicond. Sci. Technol.* **20**, S22–S34 (2005)
2. Kavcar, N., Carter, M.J., Hill, R.: Characterization of CuInSe₂ thin films produced by thermal annealing of stacked elemental layers. *Sol. Energy Mater. Sol. Cells* **27**, 13–23 (1992)
3. Pawar, B., Cai, G., Ham, D., Mane, R.S., Ganesh, T., Ghule, A., Sharma, R., Jadhava, K.D., Han, S.H.: Preparation of transparent and conducting boron-doped ZnO electrode for its application in dye-sensitized solar cells. *Solar Energy Mater. Solar Cells* **93**, 524–527 (2009)
4. Reddy, N.K., Ahsanulhaq, Q., Kim, J.H., Hahn, Y.B.: Behavior of n-ZnO devices at higher temperatures. *Appl. Phys. Lett.* **92**, 3127 (2008)
5. Sheini, F.J., Joag, D.S., More, M.A., Singh, J., Srivasatva, O.N.: Low temperature growth of aligned ZnO nanowires and their application as field emission cathodes. *Mater. Chem. Phys.* **120**, 691–696 (2010)
6. Fan, H.J., Scholz, R., Dadgar, A., Krost, A., Zacharias, M.: A low-temperature evaporation route for ZnO nanoneedles and nanosaws. *Appl. Phys.* **80**, 457–460 (2005)
7. Chena, Y.J., Zhub, C.L., Xiao, G., Chena, Y.J., Zhub, C.L., Xiao, G.: Hydrogen monitoring for power plant applications using SiC sensors. *Sens. Actuators B* **129**, 639–642 (2008)
8. Wang, X.D., Summers, C.J., Wang, Z.L.: Large-scale hexagonal-patterned growth of aligned ZnO nanorods for nano-optoelectronics and nanosensor arrays. *Nano Lett.* **4**, 423–427 (2003)
9. Kong, X.Y., Ding, Y., Yang, R., Wang, Z.L.: Single-crystal nanorings formed by epitaxial self-coiling of polar nanobelts. *Science* **303**, 1348–1351 (2004)
10. Kong, X.Y., Wang, Z.L.: Spontaneous polarization-induced nanohelices, nanosprings, and nanorings of piezoelectric nanobelts. *Nano Lett.* **3**, 1625–1631 (2003)
11. Wang, X.D., Summers, C.J., Wang, Z.L.: Mesoporous single crystal ZnO nanowires epitaxially sheathed with Zn₂SiO₄. *Adv. Mater.* **16**, 1215–1218 (2004)
12. Shi, L., Hao, Q., Yu, C., Mingo, N., Kong, X., Wang, Z.L.: Thermal conductivities of individual tin dioxide nanobelts. *Appl. Phys. Lett.* **84**, 2638–2640 (2004)
13. Roy, S., Sarkar, C.K., Bhattacharyya, P.: A highly sensitive methane sensor with nickel alloy microheater on micromachined Si substrate. *Solid State Electron.* **76**, 84–90 (2012)
14. Kim, H., Sigmund, W.: ZnO nanocrystals synthesized by physical vapor deposition. *Nanotechnology* **4**, 275–278 (2004)
15. Wen, X., Fang, Y., Pang, Q.C.Y., Wang, J., Ge, W., Wong, K.S., Yang, S.: 2-aminothiazole as a novel kinase inhibitor template. *J. Phys. Chem. B* **109**, 15303–15308 (2005)
16. Wu, C.L., Chang, L., Chen, H.G., Lin, C.W., Chang, T.F., Chao, Y.C., Yan, J.K.: Growth and characterization of chemical-vapor-deposited zinc oxide nanorods. *Thin Solid Films* **498**, 137–141 (2006)
17. Yu, H., Zhang, Z., Han, M., Hao, X., Zhu, F.: A general low-temperature route for large-scale fabrication of highly oriented ZnO nanorod/nanotube arrays. *J. Am. Chem. Soc.* **127**, 2378–2379 (2005)
18. Dalui, S., Das, S.N., Roy, R.K., Gayen, R.N., Pal, A.K.: Synthesis of DLC films with different sp²/sp³ ratios and their hydrophobic behaviour. *Thin Solid Films* **5**, 516–519 (2008)
19. Bagnall, D.M., Chen, Y.F., Zhu, Z., Yao, T., Koyama, S., Shen, M.Y., Goto, T.: Optically pumped lasing of ZnO at room temperature. *Appl. Phys. Lett.* **70**, 2230–2232 (1997)
20. Kumar, K.B., Raji, P.: Synthesis and characterisation of nano zinc oxide by sol gel spin coating II. *Recent Res. Sci. Technol.* **3**, 48–52 (2011)
21. Mondal, A., Mukherjee, N., Bhar, S.K.: Galvanic deposition of hexagonal ZnO thin films on TCO glass substrate. *Mater. Lett.* **60**, 1748–1752 (2006)
22. Khan, Z.R., Khan, M.S., Zulfequar, M., Khan, M.S.: Optical and structural properties of ZnO thin films fabricated by sol–gel method. *Mater. Sci. Appl.* **2**, 340–345 (2011)
23. Yan, F., Wang, Y., Zhang, Lin, Z., Zheng, J., Huang, J.F.: Schottky or Ohmic metal–semiconductor contact: influence on photocatalytic efficiency of Ag/ZnO and Pt/ZnO model systems. *Chem. Sus. Chem.* **7**, 101–104 (2014)
24. Ali, S.M., Farooq, W.A., Baig, M.R., Shar, M.A., Atif, M., Alghamdi, S.S., Algarawi, M.S., UR-Rehman, N., Aziz, M.: Structural and optical properties of pure and Ag doped ZnO thin



- films obtained by sol gel spin coating technique. *Mater. Sci. Pol.* **33**, 601–605 (2015)
25. Zheng, Y., Zheng, L., Zhan, Y., Lin, X., Zheng, Q., Wei, K.: Ag/ZnO heterostructure nanocrystals: synthesis, characterization, and photocatalysis. *Inorg. Chem.* **46**, 6980–6986 (2007)
 26. Wu, J.J., Tseng, C.H.: Photocatalytic properties of nc-Au/ZnO-nanorod composites. *Appl. Catal. B Environ.* **66**, 51–57 (2006)
 27. Basu, S., Dutta, A.: Studies on ZnO/p-Si heterojunctions fabricated by a modified CVD method. *Phys. Stat. Sol.* **136**, 267–272 (1993)
 28. Bhattacharyya, P., Basu, P.K., Mukherjee, N., Mondal, A., Saha, H., Basu, S.: Deposition of nanocrystalline ZnO thin films on p-Si by novel galvanic method and application of the heterojunction as methane sensor. *J. Mater. Sci. Mater. Electron.* **18**, 823–829 (2007)
 29. Mishra, G.P., Sengupta, A., Maji, S., Sarka, S.K., Bhattacharyya, P.: The effect of catalytic metal contact on methane sensing performance of nanoporous ZnO–Si heterojunction. *Int. J. Smart Sens. Intell. Syst.* **3**, 273–291 (2010)
 30. Basu, P.K., Bhattacharyya, P., Saha, N., Saha, H., Basu, S.: The superior performance of the electrochemically grown ZnO thin films as methane sensor. *Sens. Actuators B Chem.* **133**, 57–363 (2008)
 31. Ya-Bin, Z., Wei, H., Jie, N., Fan, H., Yue-Liang, Z., Cong, C.: PEDOT:PSS Schottky contacts on annealed ZnO films. *Chin. Phys. B* **20**, 047301 (2011)
 32. Wang, Z.L.: Zinc oxide nanostructures: growth, properties and applications. *J. Phys. Condens. Matter.* **16**, 829–858 (2004)

